

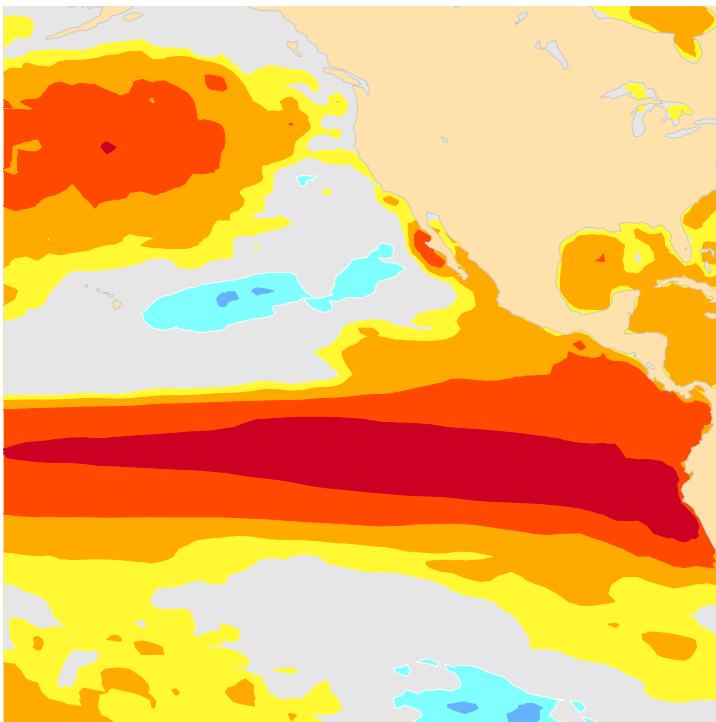
ECMWF Feature article

from Newsletter Number 176 – Summer 2023



EARTH SYSTEM SCIENCE

IFS upgrade brings many improvements and unifies medium-range resolutions



This article appeared in the Earth system science section of ECMWF Newsletter No. 176 – Summer 2023, pp. 21–28.

IFS upgrade brings many improvements and unifies medium-range resolutions

Simon Lang, Dinand Schepers, Mark Rodwell

An upgrade of ECMWF's Integrated Forecasting System (IFS) was implemented on 27 June 2023. One highlight is a horizontal resolution increase of the medium-range ensemble (ENS) to TCo1279 (9 km), which brings it to the same resolution as the high-resolution forecast (HRES). In addition to upper-air score improvements, the new ENS especially improves the skill of surface variables, such as 2 m temperature and 10 m winds, and tropical cyclones. The number of ensemble members for the extended-range ensemble forecast has increased from 51 to 101 members, and it is now run daily instead of twice weekly. These configuration changes result in substantial improvements in skill and utility for users. IFS Cycle 48r1 also benefits from a multitude of improvements to the data assimilation system as well as the forecast model, including for example higher inner-loop resolution in the data assimilation system, the assimilation of surface-sensitive microwave imager channels over land and cold ocean surfaces, and a multi-layer snow scheme in the forecast model.

Forecast model

The horizontal resolution of medium-range ensemble forecasts is increased from TCo639 (18 km) to TCo1279 (9 km). The vertical resolution remains unchanged at 137 levels. This means that the ensemble is run at the same resolution as the single HRES forecast. The horizontal resolution increase leads to improvements in forecast skill for upper-air variables and especially for surface variables. In addition, extreme events such as tropical cyclones are better represented. One consequence is that the unperturbed ENS control forecast and the HRES forecast are meteorologically equivalent and equally skilful on average. However, they can diverge on a day-to-day basis due to small technical differences and the chaotic nature of the atmosphere. In future, one of these forecasts will be retired.

An example of the impact of the horizontal resolution increase can be seen in Figure 1 for the case of severe tropical cyclone Ilsa, which made landfall over Western Australia in April 2023. The Cycle 48r1 9 km ensemble forecasts initialised on 9 April (Figure 1a) predicted Ilsa's intensity much better than the then operational 18 km ensemble forecast (Figure 1b). In addition, the 48r1 ensemble provided a more accurate track forecast.

Extended-range ensemble forecasts are now run daily instead of twice weekly, and the number of ensemble members has been increased from 51 to 101. Also, extended-range ensemble forecasts are no longer run as an extension to medium-range ensemble forecasts. Instead, they are run from initial time at a horizontal resolution of TCo319 (36 km) for the full forecast range, day 0 to 46. Hence, the horizontal resolution of the extended-range system is no longer higher for the first 15 days. Tests have confirmed that forecast scores for beyond that time do not deteriorate as a result of this change. The removal of the resolution truncation at day 15 will allow users to simplify their coding for products based on accumulated fields, such as precipitation. The extended-range forecasts are now archived in the new stream eefo, and the corresponding re-forecasts (from day 0) are now archived in the new stream eefh. The medium-range forecasts and re-forecasts remain in streams enfo and enfh, respectively. Initial condition and stochastic physics perturbations are introduced with different random numbers between medium-range and extended-range ensembles, which makes it possible to combine the two systems for forecast applications that would benefit from a larger ensemble size. In addition, the more frequent initialisation of extended-range forecasts raises the prospect of constructing lagged ensembles for this range. For more details on the extended-range upgrade, see Vitart et al. (2022).

A major change in the forecast model in Cycle 48r1 is from a single-layer to a multi-layer representation of snow in the surface scheme. The multi-layer snow scheme markedly improves the realism of the snow pack in the model and decreases the magnitude of analysis increments of snow depth. The impact on 2 m temperatures in snow-prone regions includes an improved daily cycle (Arduini et al., 2019), and there are reduced snow depth forecast errors (Figure 2).

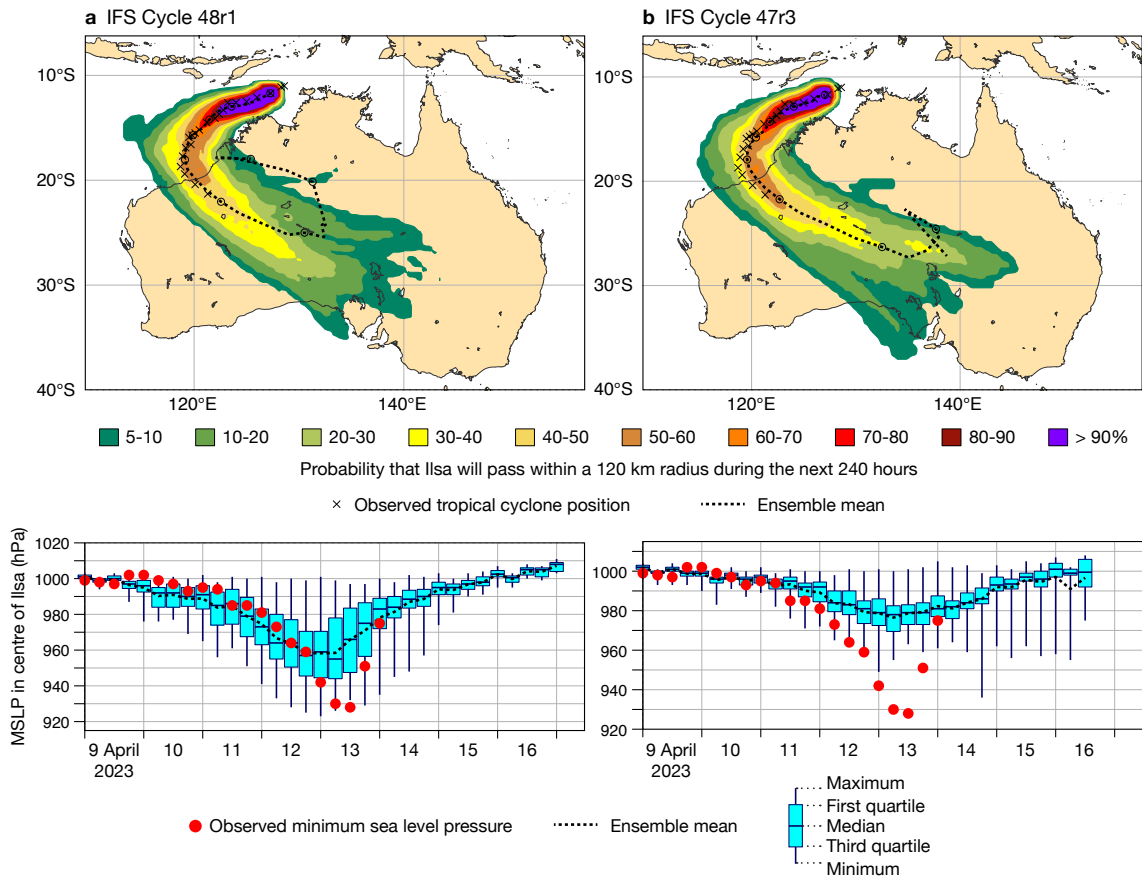


Figure 1 Tropical cyclone Ilsa, forecast from 9 April 2023, 00 UTC, in (a) the IFS Cycle 48r1 ensemble forecast with a resolution of 9 km, and (b) the IFS Cycle 47r3 ensemble forecast with a resolution of 18 km. Shown are the strike probability (top) and mean sea level pressure (MSLP) in the centre of Ilsa (bottom).

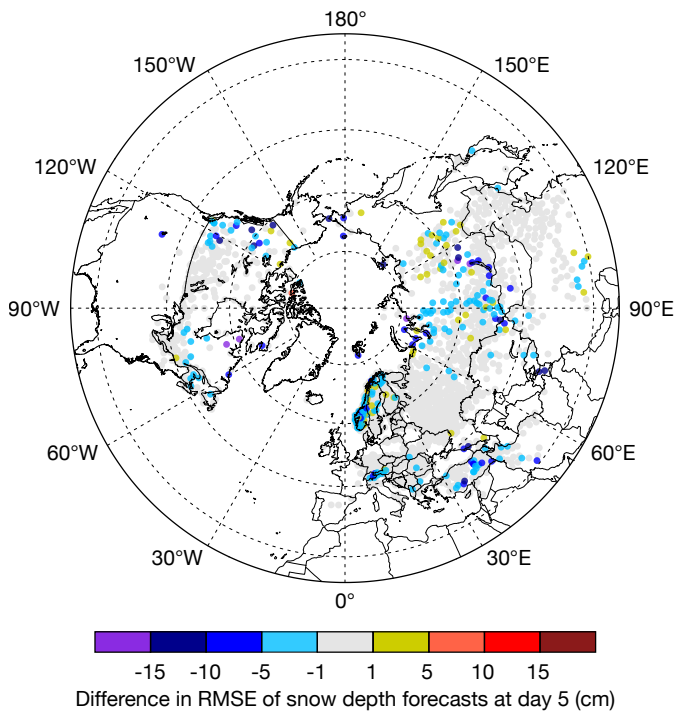


Figure 2 The figure shows the difference between multi-layer and single-layer snow in the root-mean-square error (RMSE) of snow depth forecasts at day 5, compared with SYNOP weather station values in the 2019/20 winter. Blue colours indicate an improvement when multi-layer snow is used.

Some of the IFS climate fields have been updated: the orography, the land–sea mask, lake depth and the glaciers mask. The improved climate fields increase the realism of inland water distribution and provide a more accurate surface skin temperature.

The parametrization of microphysical processes has been revised in Cycle 48r1 to allow supercooled drizzle drops to be formed and only to freeze if they come into contact with pre-existing ice or snow particles, or experience much colder temperatures. This allows the IFS to predict high-impact freezing drizzle events, where supercooled rain/drizzle drops freeze on impact at the surface and form a glaze of ice. Figure 3 shows an example case study on 19 December 2017 over Germany, where freezing drizzle was observed. The revised microphysical parametrization in Cycle 48r1 shows the occurrence of freezing drizzle in the area, while the operational forecast model at the time did not have this ability.

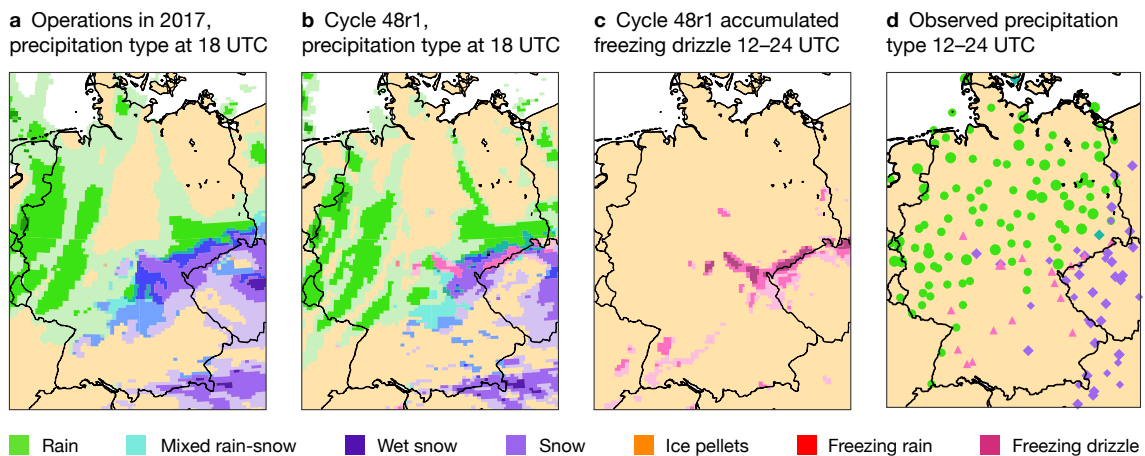


Figure 3 In this case from 19 December 2017, (a) no freezing drizzle was indicated in forecasts operational at the time, as in this short-range (18-hour) forecast, whereas (b) Cycle 48r1 predicts freezing drizzle. The locations of freezing drizzle in (c) 12–24 hour accumulations in Cycle 48r1 agrees well with (d) the observation reports over the same period. Shading indicates 0.02, 0.1 and 0.5 mm accumulated precipitation per hour in (a) and (b) and per 12 hours in (c).

The partitioning of low-level orographic drag processes to the surface drag underwent a major change, which includes revisions of the subgrid orography fields and the orographic low-level flow blocking, and gravity wave drag parametrizations. The subgrid orography fields are now representative of orographic features with scales smaller than the effective orographic resolution of the forecast model (several times the grid length) rather than only scales smaller than the grid length (Kanehama et al., 2022). There is now a shallower sponge layer at the top of the forecast model, starting at 0.7 hPa instead of 10 hPa. This leads to a more realistic gravity-wave breaking level and thus an improved gravity-wave drag profile.

A new streamlined algorithm for the computation of semi-Lagrangian advection departure points is introduced in Cycle 48r1. It is based on a scheme that is more suitable for single precision calculations near the poles, resulting in a more compact and simplified code. It requires fewer iterations to achieve the same accuracy as the previous approach. Hence, the overall cost of the scheme is reduced (Diamantakis & Váňa, 2022).

A new vertical Finite Element discretisation scheme (Vivoda et al., 2018) has been introduced in Cycle 48r1, which is applicable to both the hydrostatic and non-hydrostatic dynamical core options of the IFS and improves the conservation of the total air mass in single precision. To improve water and energy conservation properties in the IFS dynamics, global mass fixers have been activated for all moist species, including water vapour (Becker et al., 2022). Furthermore, some revisions to the saturation adjustment and ice fall speed have been made. Perturbations to the cloud saturation tendency have been removed from the Stochastically Perturbed Parametrization Tendencies scheme (SPPT) to avoid rare model instabilities. In addition to improving the underlying physical consistency of the IFS, the combined changes improve medium-range ensemble scores, especially in the tropics.

The physics–dynamics interface across the non-linear, tangent-linear and adjoint models has been made more consistent. As a result, the tangent-linear model now better approximates the full non-linear model.

Cycle 48r1 introduces the new Hybrid Linear Ozone (HLO) scheme. Some terms within the scheme are inferred from chemistry models, while others are inferred from multiple years of observationally constrained ozone reanalyses from the EU-funded Copernicus Atmosphere Monitoring Service (CAMS) implemented by ECMWF (Williams et al., 2021). The HLO scheme improves stratospheric wind forecasts. A semi-Lagrangian 2-grid-point vertical filter (SLVF) on temperature has been introduced above 100 hPa. This alleviates unphysical global-mean cooling in the stratosphere in the forecast model and improves the fit to GNSS-RO observations.

The wave model infrastructure has undergone wide-ranging optimisation, which will enable future high-resolution runs.

Data assimilation and observation usage

A major technical upgrade of the data assimilation system in Cycle 48r1 is the switch to the Object-Oriented Prediction System (OOPS). OOPS provides flexibility, which will facilitate the development of ECMWF's data assimilation capabilities in the future. In addition, it improves the scalability of the current system (English et al., 2017).

With Cycle 48r1, the Continuous Observation Processing Environment (COPE) has been introduced, which performs observation pre-processing incrementally shortly after observations are received. It is more scalable than the legacy observation processing system and will be able to scale to hundreds of billions of observations.

The resolution of the final inner loop of the 4D-Var data assimilation system is increased from TL399 (50 km) to TL511 (40 km), which enables a better fit to observations and improves forecast scores.

The radiative transfer model (Radiative Transfer for TOVS, RTTOV) used in the IFS has been upgraded to the latest version, RTTOV 13.0, bringing improved microwave radiative transfer as well as a major upgrade of cloud and precipitation optical properties (Geer et al., 2021; Barlakas et al., 2021).

In addition, the assimilation of satellite observations in the microwave spectral range has been improved by the implementation of a Lambertian representation of surface reflection over snow and ice (appearing uniformly bright from all directions of view), when previously a specular representation was used (incident radiation is reflected into a single outgoing direction) (Bormann, 2022). There are also improvements through the activation of humidity-sensitive channels of the ATMS instrument over snow-covered areas in clear-sky conditions. Selected microwave channels and sensors now employ slant-path interpolation when assimilated in the all-sky system.

An important advancement in this cycle is the assimilation of microwave imager channels over snow-free land (excluding desert surfaces), enabled by an enhanced estimation of surface emissivity appropriate for all-sky assimilation (Figure 4a). Furthermore, improved sea-ice detection now allows assimilation of surface-sensitive microwave imager observations over land and ocean in high-latitude ranges (poleward of ± 60 degrees latitude). Other refinements include the addition of microwave humidity sounding radiances over land at high latitudes, as well as a better handling and increased usage of microwave sounding observation over mixed surfaces, involving land, water and sea ice, such as in coastal and lake regions (Geer et al., 2022) (Figure 4b). These changes are a key step towards an all-sky/all-surface use of microwave radiances.

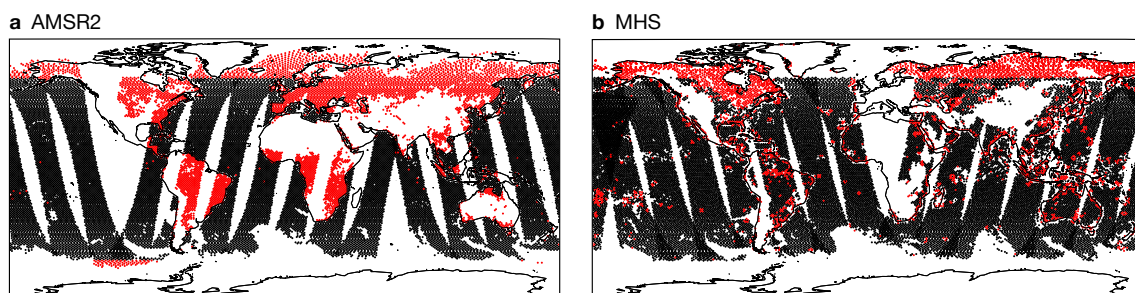


Figure 4 Example of the coverage of observations to be assimilated in Cycle 48r1 from (a) the Advanced Microwave Scanning Radiometer – 2 (AMSR2) in channel 11 (36.5 GHz v-polarised), and (b) the Microwave Humidity Sounder (MHS) on Metop-B in channel 5 (190.311 GHz), with black dots indicating data assimilated in Cycle 47r3 and red dots the data added in Cycle 48r1. Data are taken for the 00 UTC cycle on 20 June 2019.

The thinning of scatterometer observations has been significantly reduced so that the number of assimilated observations is strongly increased. This represents an important step towards a better analysis of low-level winds over sea areas, e.g. around tropical cyclones.

Additional developments have improved the assimilation of a suite of hyperspectral infrared sounders. Specifically, an improved trace gas detection scheme for identifying and rejecting soundings affected by excessive hydrogen cyanide concentrations, associated with forest fires, helps to reduce false alarms for IASI (Infrared Atmospheric Sounding Interferometer) and AIRS (Atmospheric Infrared Sounder). An upgraded aerosol-type classification now informs a channel-specific aerosol rejection algorithm over sea areas. Ozone-sensitive CRIS (Cross-track Infrared Sounder) channels are bias-corrected taking into account the type of air-mass, bringing the approach into line with that used for similar channels on AIRS and IASI.

Impact on medium- and extended-range forecasts

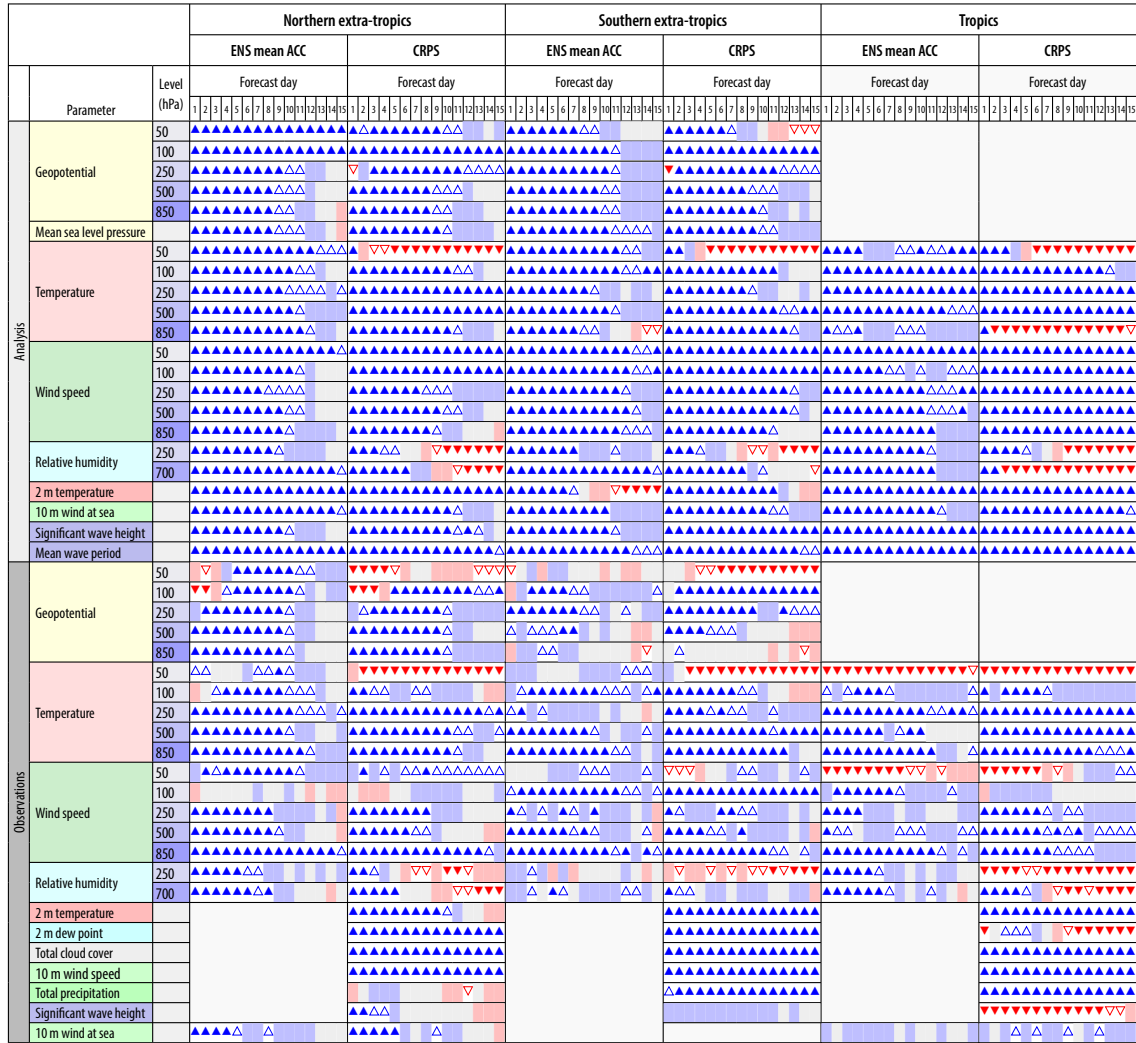
The scorecard summarising the ENS score changes is shown in Figure 5. Most ENS scores of surface variables, such as 2 m temperature, 10 m wind and total precipitation, are markedly improved, in the range of 2% to 6%. Most upper-air variables are improved as well, by around 1% to 3%. Stratospheric winds are improved, but some degradations of stratospheric temperatures due to increased biases can be observed. There are also pronounced improvements in scores over the Arctic and Antarctic, partly associated with the increased spread generated by the multi-layer snow scheme (not shown). The ensemble spread of upper-air variables (ensemble standard deviation, not shown) is reduced in the mid-latitudes (by around 1% to 2%) but mainly increased in the tropics (by around 2% to 3%), and the ensemble spread of surface variables is increased (by around 2% to 6%).

Cycle 48r1 improves ENS tropical cyclone track and intensity forecasts, with position errors reduced by up to 10% (Figure 6a,b) and core pressure errors reduced by around 20% (Figure 6c,d). The reduced track errors are mainly associated with a reduced slow-propagation bias of the forecast model. The intensity forecast is improved because the higher horizontal resolution allows for a better representation of the strong horizontal gradients associated with intense systems like tropical cyclones. This is also reflected in the strongly increased intensity spread of the ENS. The track spread, on the other hand, is very similar to that of the previous cycle (not shown).

The scores of the HRES forecast are summarised in Figure 7. These show clear overall improvements. Upper-air troposphere scores are improved by around 1% to 3% in the northern hemisphere and in the tropics. In line with the ENS, stratospheric winds are improved, but some degradations of stratospheric geopotential can be observed due to increased biases. These impacts are mainly related to the new HLO scheme. Upper-level Arctic and Antarctic scores are improved, in line with the ENS scores.

Surface winds in the tropics appear degraded when verified against ECMWF's analysis. This apparent degradation is caused by the large increase of scatterometer observations and the associated decorrelation of analysis and forecast errors. Verification against observations does not show the degradation. HRES northern and southern hemisphere 2 m temperature scores also show some degradation, which comes from increased (more realistic) analysis and forecast activity generated by the multi-layer snow scheme. Tropical cyclone track and intensity forecast scores in HRES are very similar to those for the previous cycle.

The forecast model changes result in small improvements of the weekly mean extended-range scores. However, the increased ensemble size of the extended-range system, as well as the increased run frequency (daily instead of twice weekly), lead to substantial skill improvements (Vitart et al., 2022).



Symbol legend: for a given forecast step...

- ▲ 48r1 better than 47r3 statistically significant with 99.7% confidence
- △ 48r1 better than 47r3 statistically significant with 95% confidence
- 48r1 better than 47r3 statistically significant with 68% confidence
- no significant difference between 47r3 and 48r1
- 48r1 worse than 47r3 statistically significant with 68% confidence
- ▽ 48r1 worse than 47r3 statistically significant with 95% confidence
- ▼ 48r1 worse than 47r3 statistically significant with 99.7% confidence

Figure 5 This ENS scorecard compares IFS Cycle 48r1 with IFS Cycle 47r3 for the anomaly correlation coefficient (ACC) of the ensemble mean and the Continuous Ranked Probability Score (CRPS). It shows predominantly improvements (blue colours) and a few deteriorations (red colours). Results are verified by the respective analyses and observations at 00 and 12 UTC, based on about 550 forecast runs in the period June 2020 – April 2023.

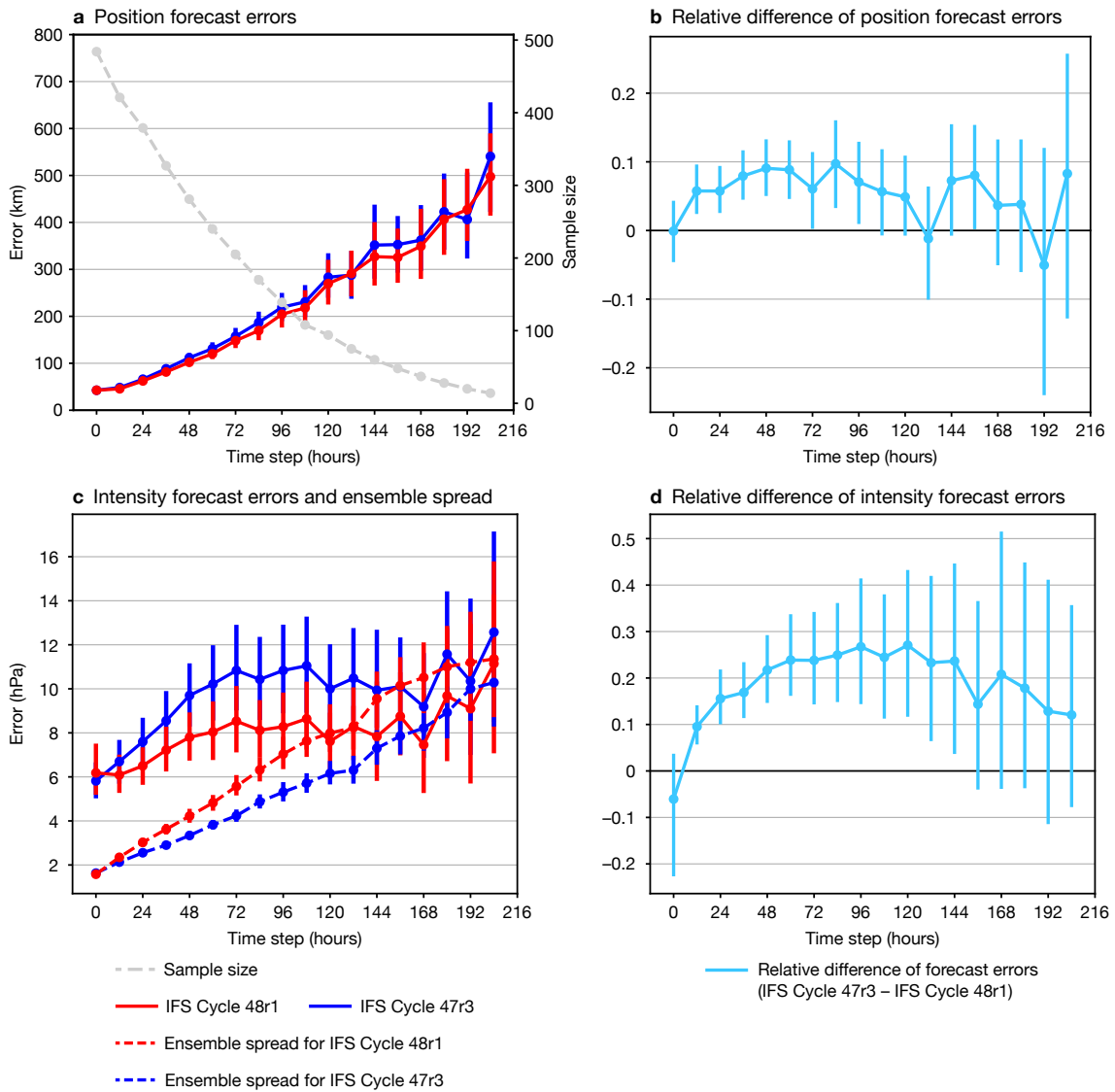


FIGURE 6 ENS tropical cyclone position and intensity forecast errors in IFS Cycle 48r1 compared to IFS Cycle 47r3, showing (a) position forecast errors of Cycle 48r1 and Cycle 47r3, (b) the relative difference of position forecast errors, with positive values showing improved forecast errors for Cycle 48r1, (c) intensity (central pressure) forecast errors (solid lines) and ensemble spread (dashed lines) of Cycle 48r1 and Cycle 47r3, and (d) the relative difference of intensity forecast errors, with positive values showing improved forecast errors for Cycle 48r1. The vertical error bars represent 95% confidence intervals.

New products

There is an additional precipitation type (see WMO Table 4.201) to indicate the occurrence of freezing drizzle at the specified output time, as explained above (Figure 3). Cycle 48r1 also contains new parameter outputs for ‘most-frequent’ and ‘most-severe’ precipitation type in the last 1, 3 or 6 hours to complement the instantaneous precipitation type parameter.

Summary

IFS Cycle 48r1 brings many improvements and innovations for both the forecast model and the observation handling and data assimilation system. It introduces several important technical developments, like OOPS and COPE, and optimisation to future-proof the wave model. It also increases observation counts, for example of scatterometer observations, and it improves the data assimilation system, for example by the 4D-Var inner-loop resolution increase from TL399 to TL511, improving analysis accuracy. It has, among other things, a new multi-layer snow model for a more realistic representation of snow, the new Hybrid Linear Ozone scheme, and improvements to the dynamics which lead to markedly improved water and energy conservation properties of the forecast model. The combined data assimilation and model changes significantly improve forecast skill.

The extended-range system benefits from an increase in ensemble size, from 51 to 101 members. The daily initialisation of the extended-range system means that there are now up-to-date forecasts available at all times, instead of forecasts that can be several days old.

The horizontal resolution upgrade of the ENS from 18 to 9 km is a major step forward and brings it to the same resolution as the HRES forecast. In the future, the HRES forecast and the unperturbed control forecast of the ensemble will be merged. The resolution upgrade leads to marked improvements of upper-level scores and greatly improves forecast skill for surface variables, such as 2 m temperature and 10 m winds, and for extreme events, such as tropical cyclones.

Further reading

- Arduini, G., G. Balsamo, E. Dutra, J.J. Day, I. Sandu, S. Boussetta et al.**, 2019: Impact of a multi-layer snow scheme on near-surface weather forecasts. *Journal of Advances in Modeling Earth Systems*, **11**, 4687–4710. <https://doi.org/10.1029/2019MS001725>
- Barlakas, V., A.J. Geer & P. Eriksson**, 2021. Introducing hydrometeor orientation into all-sky microwave and submillimeter assimilation. *Atmospheric Measurement Techniques*, **14**(5), 3427–3447.
- Becker, T., T. Rackow, X. Pedruzo, I. Sandu, R. Forbes, M. Diamantakis et al.**, 2022: Fixing water and energy budget imbalances in the Integrated Forecasting System, *ECMWF Newsletter No. 172*, 14–15. <https://shorturl.at/BGOR6>
- Bormann, N.**, 2022. Accounting for Lambertian reflection in the assimilation of microwave sounding radiances over snow and sea-ice. *Quarterly Journal of the Royal Meteorological Society*, **148**(747), 2796–2813.
- Diamantakis, M. & F. Váňa**, 2022: A new way of computing semi-Lagrangian advection in the IFS. *ECMWF Newsletter No. 173*. <https://doi.org/10.21957/md5f8jx27p>
- English, S., D. Salmond, M. Chrust, O. Marsden, A. Geer, E. Holm et al.**, 2017: Progress with running IFS 4D-Var under OOPS, *ECMWF Newsletter No. 153*, pp. 13–14. <https://www.ecmwf.int/en/newsletter/153/news/progress-running-ifs-4d-var-under-oops>
- Geer, A.J., K. Lonitz, D.I. Duncan & N. Bormann**, 2022: Improved surface treatment for all-sky microwave observations. *ECMWF Technical Memorandum No. 894*. <https://doi.org/10.21957/zi7q6hau>
- Geer, A.J., P. Bauer, K. Lonitz, V. Barlakas, P. Eriksson, J. Mendrok et al.**, 2021. Bulk hydrometeor optical properties for microwave and sub-millimetre radiative transfer in RTTOV-SCATT v13. 0. *Geoscientific Model Development*, **14**(12), 7497–7526.
- Kanehama, T., I. Sandu, A. Beljaars, A. van Niekerk, N. Wedi, S. Boussetta et al.**, 2022: Evaluation and optimization of orographic drag in the IFS, *ECMWF Technical Memorandum, No. 893*. <https://doi.org/10.21957/fps6gngqe>
- Vitart, F., M.A. Balmaseda, L. Ferranti & M. Fuentes**, 2022: The next extended-range configuration for IFS Cycle 48r1. *ECMWF Newsletter No. 173*. <https://doi.org/10.21957/fv6k37c49h>
- Vivoda, J., P. Smolikova, & J. Simarro**, 2018: Finite Elements Used in the Vertical Discretization of the Fully Compressible Core of the ALADIN System, *Monthly Weather Review*, **146**. <https://doi.org/10.1175/MWR-D-18-0043.1>
- Williams, R., R. Hogan, I. Polichtchouk, M. Hegglin, T. Stockdale & J. Flemming**, 2021: Evaluating the impact of prognostic ozone in IFS NWP forecasts. *ECMWF Technical Memorandum, No. 887*. <https://doi.org/10.21957/rakfo1qo3>

© Copyright 2023

European Centre for Medium-Range Weather Forecasts, Shinfield Park, Reading, RG2 9AX, UK

The content of this document, excluding images representing individuals, is available for use under a Creative Commons Attribution 4.0 International Public License. See the terms at <https://creativecommons.org/licenses/by/4.0/>. To request permission to use images representing individuals, please contact pressoffice@ecmwf.int.

The information within this publication is given in good faith and considered to be true, but ECMWF accepts no liability for error or omission or for loss or damage arising from its use.